

Spatially Resolved Potential Distribution in Carbon Nanotube Cross-Junction Devices

By Eduardo J. H. Lee,* Kannan Balasubramanian, Marko Burghard, and Klaus Kern

Owing to their outstanding electrical and optical properties, SWCNTs are promising building blocks for various applications, in particular molecular electronics.^[1] Field-effect transistors (FETs) comprising an individual semiconducting nanotube (CNFETs) as the channel were first demonstrated a decade ago.^[2] Although these devices have since become a topic of intense research, the widespread application of carbon nanotubes (CNTs) in electronics has so far been hampered by the lack of reliable methods to exclusively synthesize or separate semiconducting CNTs. First steps towards this objective have only recently been made.^[3] In parallel, FETs composed of networks or thin films of CNTs have been developed, which offer several advantages over individual CNTs, most prominently easier fabrication and higher operation currents.^[4] In this case, the electrical response is an ensemble average over the properties of the metallic and semiconducting CNTs that constitute the transistor channel. FETs with carrier mobilities of the order of $10\text{--}100\text{ cm}^2\text{ V}^{-1}\cdot\text{s}^{-1}$ and ON/OFF ratios exceeding 10^5 have been realized from CNT networks of sufficiently low density to prevent the formation of metallic percolating paths inside the channel.^[4] Moreover, network devices also hold promise for applications in flexible electronics^[5] and optoelectronic devices, such as light detectors and light emitters.^[6] While the good performance of such FETs renders them technologically attractive, the mechanisms involved in the electrical transport in the constituent networks are still poorly understood.

The basic components of such networks/films are CNT crossings, which can be classified as of M-M, M-S, and S-S type, where M and S stand for metallic and semiconducting CNTs, respectively. While the presence of Schottky barriers at M-S crossings is well-documented from charge transport studies,^[7] only indirect proof has been obtained for the presence of p-p isotype heterojunctions at S-S crossings between CNTs with different bandgaps, as in most cases the investigated devices comprised contacts and intertube crossings with high resistance.^[8] In the work presented here, we performed a systematic investigation of different types of cross-junction devices using

scanning photocurrent microscopy (SPCM). This method has been first demonstrated on individual S- and M-CNTs,^[9] and subsequently been used to probe electric field modulations along individual S-CNTs in different types of devices.^[10]

We start by addressing the photoelectric behavior of low-density random CNT networks. Figure 1a displays an atomic force microscopy (AFM) image of a typical network device, which exhibited unipolar p-type character with an ON/OFF ratio of approximately 10^4 . While ambipolarity is commonly observed in CNFETs comprising individual tubes with relatively large diameter, the unipolar character of the network indicates that there is at least one tube in the electrical path with a large bandgap. SPCM images acquired under zero drain-source bias, as exemplified in Figure 1b, exhibit a number of photocurrent lobes distributed throughout the network. As demonstrated by SPCM studies on individual nanotubes,^[9,10] photocurrent responses are generated by the dissociation of photoexcited electron-hole pairs at local electric fields, thus revealing the position of transport barriers. By comparison with the corresponding AFM image, it can be discerned that in the ON state (gate-source voltage $V_{\text{gs}} = -10\text{ V}$), the photocurrent signals are located at the electrical contacts and at the nanotube-nanotube crossings. While the photoresponses detected at the contacts can be directly attributed to potential barriers at the metal/nanotube interfaces,^[9,10] the nature of the responses observed at the crossings is addressed by the experiments described below. Curiously, in the OFF state ($V_{\text{gs}} = 10\text{ V}$) the photocurrent lobes at the contacts disappear, and the photoresponse is given by just a few of the crossed-nanotube junctions. Furthermore, when a drain-source bias is applied to the device (Fig. 1c), the photoresponse narrows down to one or at most a few spots within the network (Supporting Information).^[11] Such behavior has been consistently observed on more than 15 low-density samples, which underscores the determining role of the intertube junctions in the response of nanotube networks. It further demonstrates that, under applied bias, local electric fields are present at only a few of the constituting cross junctions, and hence the electrostatic potential drops predominantly at these positions within the device. Such localized photoconductive response within a nanotube network is in contrast to earlier studies, which assumed that the entire network would contribute to the generated photocurrent.^[6a,6b] In order to illuminate the origin of the aforementioned photocurrent phenomena and its implication for the electrical transport through such networks, we investigated model devices comprising single crossings between individually characterized nanotubes.

Figure 2a shows an AFM image of a typical device comprising a CNT cross junction. In most of our devices, each SWCNT could be

[*] E. J. H. Lee, Dr. K. Balasubramanian, Dr. M. Burghard, Prof. K. Kern
Max Planck Institute for Solid State Research
Heisenbergstrasse 1
70569 Stuttgart (Germany)
E-mail: e.lee@fkf.mpg.de
Prof. K. Kern
Institut de Physique des Nanostructures
École Polytechnique Fédérale de Lausanne (EPFL)
1015 Lausanne (Switzerland)

DOI: 10.1002/adma.200803545

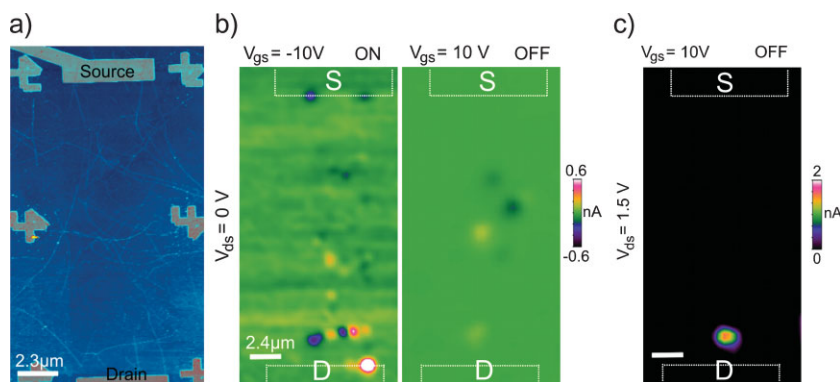


Figure 1. Photocurrent response of a nanotube network device. a) AFM image of a device comprising a low-density random CNT network. b) Zero-bias SPCM image of the same device recorded in the p-type ON ($V_{gs} = -10$ V) and OFF ($V_{gs} = 10$ V) states. c) Photocurrent map acquired in the OFF state under applied bias ($V_{ds} = +1.5$ V). The localization of the photoconductive response around one dominant crossed-nanotube junction is clearly observed.

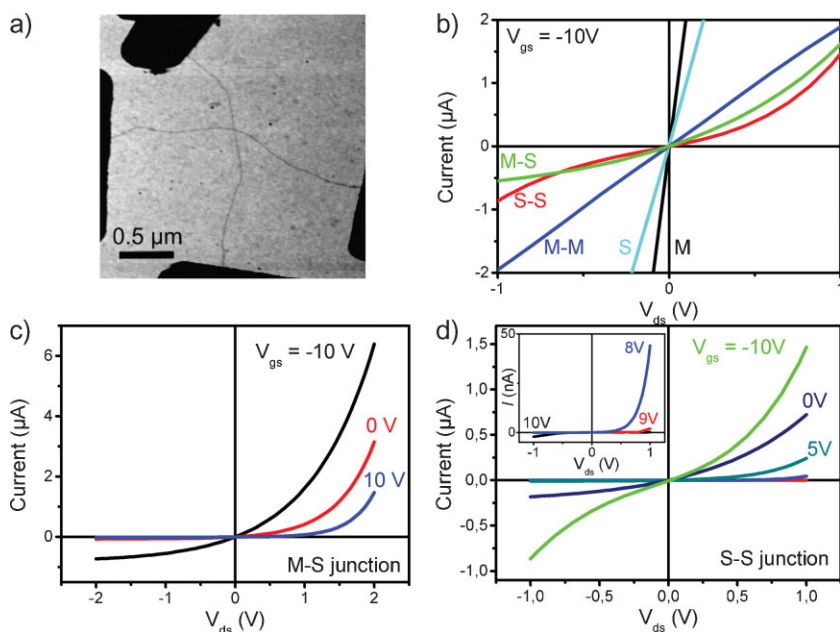


Figure 2. Electrical characterization of crossed-nanotube-junction devices. a) AFM image of a typical cross-junction device. b) Current-voltage characteristics, taken with $V_{gs} = -10$ V, of M- and S-CNTs that constitute cross-junction devices. The electrical responses of M-M, M-S and S-S junction devices are added for comparison. c) Gate-voltage-dependent electrical response of a M-S cross-junction device. d) Gate-voltage-dependent I - V curves of a S-S junction device. The inset highlights the response observed in the OFF state.

accessed by two electrodes and thus individually characterized prior to SPCM measurement. On the other hand, in cases where space constraints prevented such electrode attachment, electrical characterization was achieved by defining additional electrodes after collecting the SPCM data. Electrical and SPCM measurements on these devices were performed in two-terminal configuration while the remaining electrodes were kept at floating potential, enabling us either to investigate the constituting M- and S-CNTs individually, or to measure the response

across the intertube crossings. Figure 2b shows that the current-voltage (I - V) characteristics of individual M and S nanotubes are not significantly affected by a second crossing tube, as is apparent from their linear response at low bias. The I - V curves measured across the different types of intertube crossings are included in the figure for comparison. All types of junctions display a considerable resistance increase, which can be partially attributed to the presence of a tunneling barrier between the two crossed tubes. Moreover, while the electrical response of the M-M junction device is ohmic, the M-S and S-S junctions exhibit nonlinear responses. Detailed gate-voltage-dependent I - V traces measured across the M-S and S-S junctions are shown in Figures 2c and d, respectively. The M-S junction device displays strong current rectification, with a gate-induced modulation of the $I_{\text{forward}}/I_{\text{reverse}}$ ratio between 5 and ca. 10^4 . The S-S junction device, on the other hand, exhibits a diode-like rectification only in the OFF state, where $I_{\text{forward}}/I_{\text{reverse}}$ is ca. 10^2 . The reverse current is considerably increased in the ON state, such that the device behaves as a leaky diode.

SPCM was subsequently employed to investigate the photoelectric response of the crossed-nanotube-junction devices. Photocurrent maps acquired at zero drain-source bias from M-M, S-S, and M-S junction devices in the ON state ($V_{gs} = -10$ V) are presented in Figure 3 along with the corresponding optical reflection images (left-hand column, where dashed lines indicate the position of the tubes). In the case of the M-S junction device, the longer nanotube, which is connected to two electrodes, is metallic. The middle column in Figure 3 displays photocurrent images measured through individual nanotubes within the different devices. In all three cases, both the M- and S-CNTs show enhanced photoresponses at the metal contacts, similar to previous SPCM studies on individual nanotubes.^[9,10] Interestingly, no significant photoresponses occur at the crossing points, in accordance with the above conclusion that the underlying nanotube is only weakly disturbed by the second crossing tube. The

images in the right-hand column of Figure 3 represent the responses measured across the different junctions. While both M-M and S-S devices display strong photoresponses at the metal contacts, a sizeable photocurrent signal at the intertube crossing appears only in the latter device. The negligible photoresponse at the M-M junction evidences the absence of a potential barrier, which is in agreement with the ohmic behavior in the I - V characteristics of the corresponding device. The signal at the intertube crossing within the S-S junction device reflects the

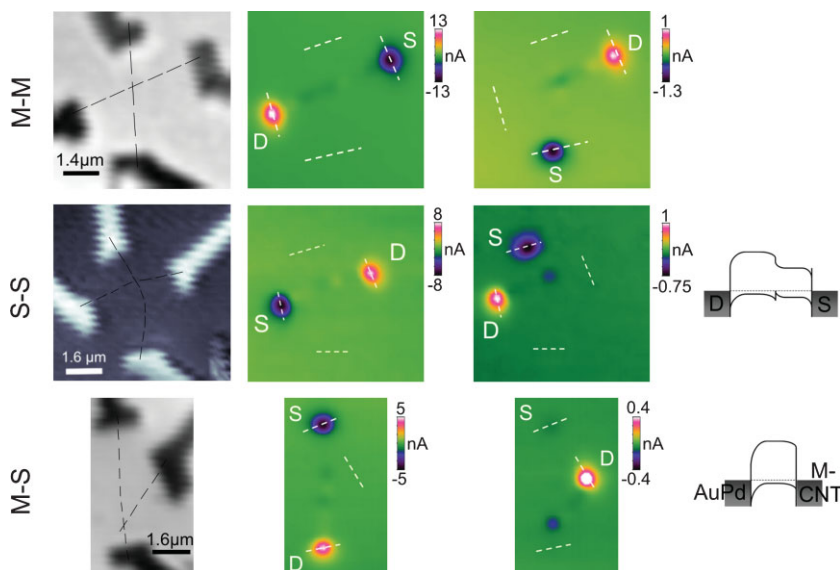


Figure 3. Zero drain–source bias SPCM characterization of M-M, M-S, and S-S cross-junction devices. Measurements were taken with $V_{gs} = -10$ V (p-type ON state). The optical reflection images of the devices are shown in the left-hand column, where the dashed black lines mark the position of the nanotubes. The longer nanotube in the M-S junction device is metallic. Photocurrent images were measured through the individual constituting M- and S-CNTs (middle column) or across the intertube junctions (right-hand column). The band diagram schemes in the lower right corner depict S-S and M-S cross-junction devices.

formation of an isotype p-p heterojunction due to the CNT bandgap difference. This conclusion is corroborated by the observation of stronger photoresponses at the junction for larger diameter differences between the crossing nanotubes (Supporting Information). On the other hand, in the case of the M-S device, the photocurrent signal detected at the intertube crossing originates from the Schottky barrier present at that position. The fact that this signal is of lower intensity than that detected at the metal (drain) contact to the S-CNT is consistent with the lower work function difference between prototypical S- and M-CNTs ($\Phi_{AuPd} \approx 4.7 \pm 0.2$ eV),^[12] as compared to the interface between S-CNTs and AuPd ($\Phi_{AuPd} \approx 5.1$ eV). In conclusion, the M-S device largely behaves like an asymmetrically contacted S-CNT with a dominant built-in electric field close to the AuPd electrode. The electrostatic potential profiles of the M-S and S-S junctions (Supporting Information), derived from the photocurrent distribution, agree remarkably well with generally accepted models for asymmetric CNFETs or S-S CNT heterojunction devices.^[8,13] Furthermore, it is concluded that the zero-bias photoresponses at nanotube crossings in network devices (Fig. 1b) can be ascribed to semiconducting heterojunctions and Schottky barriers located at S-S and M-S crossings, respectively.

The gate dependence of the zero-bias photocurrent response, presented in Figure 4, reveals that the magnitude of the photocurrent responses at the metal contacts decreases upon switching the devices from the p-type ON to the OFF state. Such a behavior has been previously observed in individual CNTs and reflects the flattening of the nanotube bands at the contacts, as the Fermi level of the CNT is shifted. By contrast, the magnitude of the photocurrent signal at the intertube crossing changes to a smaller extent, indicating that the built-in electric field at the

nanotube-nanotube interface is only weakly affected by the gate voltage, as expected from the simultaneous shift of the Fermi level of both M- and S-CNTs. Hence, while the electric fields associated with the barriers at the metal contacts decrease considerably when approaching the OFF state, those located at the intertube crossings remain largely unaffected, as illustrated by the schematic band diagrams in Figure 4. From these, it can be concluded that the role of intertube crossings becomes more important in the OFF state, in agreement with the observed photoresponse of nanotube network devices (Fig. 1b).

Further insight into the properties of the M-S and S-S intertube crossings was gained from gate-voltage-dependent SPCM measurements under application of a fixed drain–source bias. Such images acquired around the OFF state of the M-S junction device of Figure 3 ($V_{ds} = 0.8$ V), are presented in Figure 5a, where it can be seen that the photocurrent generation is restricted to the semiconducting nanotube, independent of the gate voltage. In the n-type regime ($V_{gs} = 10$ V), the photocurrent is concentrated in the vicinity of the M-S junction, where the metallic tube

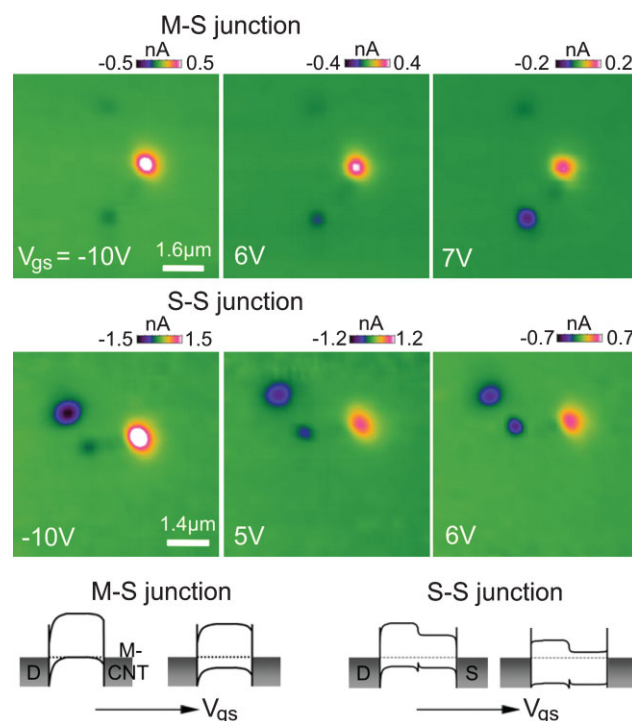


Figure 4. Gate-voltage-dependent zero-bias SPCM response of cross-junction devices. Photocurrent maps of the M-S and S-S junction devices shown in Figure 2 as a function of the gate voltage. The band diagram schemes illustrate the effect of the gate voltage on the relative magnitude of the electric fields at the contacts and the intertube crossings. The devices are switched from the ON to the OFF state with increasing V_{gs} .

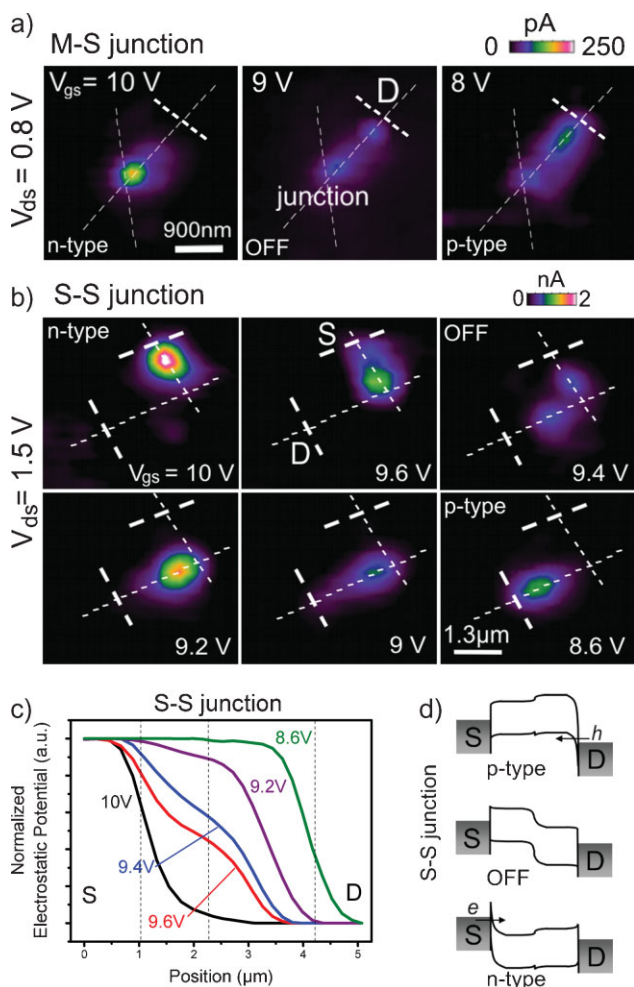


Figure 5. Photocurrent response under applied drain–source bias. Gate-voltage-dependent SPCM measurements taken under an applied bias for a) a M-S ($V_{ds} = 0.8$ V) and b) a S-S ($V_{ds} = 1.5$ V) cross-junction device. The thick white dashed lines mark the position of the source and drain electrical contacts, whereas the thin dashed lines indicate the position of the nanotubes. c) Normalized electrostatic potential profiles obtained from the photocurrent images in (b). d) Schematic illustration of the operating mechanism of the S-S cross junction. In the OFF state, the electrostatic potential drops predominantly at the intertube junction.

can be viewed as source contact to the semiconducting tube, since the potential drop along the former is comparatively small, as indicated by its negligible photoresponse. Upon moving towards the p-type regime ($V_{gs} = 8$ V), the photocurrent response progressively shifts towards the drain contact. This behavior closely resembles that of individual S-CNTs,^[10a] and is in agreement with the theoretically predicted changes in the electrostatic potential profile induced by gate voltage modulation.^[14] It further consolidates that M-S junction devices effectively represent S-CNTs with asymmetric Schottky contacts, which accounts for the diode character of these devices.^[13] The photoresponse of the S-S junction device ($V_{ds} = 1.5$ V) of Figure 3 is illustrated in Figure 5b, as it is switched from the n- to the p-type regime. Like for the M-S junction device, the photocurrent is seen to be localized around the source contact in the n-type

regime, and upon switching from the n- to p-type regime, it is gradually shifted to the drain contact. In the OFF state ($V_{gs} = 9.4$ V) the photoresponse occurs almost symmetrically around the S-S junction, whereas it is absent at the electrical contacts. The corresponding electrostatic potential profiles extracted from the photocurrent distribution (Fig. 5c) reveal that, in the ON states of the device, the applied bias drops predominantly in the vicinity of the contacts, while there is only a slight potential drop at the heterojunction. On this basis, we attribute the nonlinear electrical response in the ON state of the device (Fig. 2d) to the asymmetry of the contacts. In the OFF state, by contrast, the applied potential predominantly drops at the semiconducting heterojunction. Under this condition, the device displays a diode-like behavior (inset of Fig. 2d), as typically observed for devices comprising heterojunctions.^[8,15] The overall behavior is schematically illustrated by the band profiles in Figure 5d, which highlight the existence of two different transport modes controlled by the gate. Specifically, in the contact-dominated ON states the contact barriers are thinned, thereby enhancing charge carrier injection by tunneling, in a similar manner as observed for individual S-CNT devices. In comparison, the heterojunction-dominated OFF state is characterized by pronounced current rectification at sufficiently large drain–source bias.

The above SPCM results demonstrate that potential barriers located at nanotube crossings become dominant in the OFF state of cross-junction devices, as a result of the flattening of Schottky barriers present at the electrical contacts. Consequently, under applied bias, the electrostatic potential drop, and thus the photoresponse, occurs predominantly at these positions. While the observed photocurrent response of individual cross junctions shares many similarities with respect to that of network devices (Fig. 1), the mechanism which leads to only a few of the intertube junctions dominating the response of the networks is still unclear. In order to elucidate such behavior, further studies on devices comprising multiple cross junctions would be of great interest.

In summary, SPCM has been successfully employed to elucidate the spatial origin of photoconductivity in devices comprising crossed-nanotube junctions. Zero-bias SPCM measurements have directly evidenced the formation of isotype heterojunctions and Schottky barriers at S-S and M-S nanotube crossings, respectively. Moreover, the derived electrostatic potential profiles illustrate two transport modes for devices containing cross junctions. In the ON state, the potential profile is dominated by the electrical contacts, whereas in the OFF state, the transport is dominated by the cross junction, which imparts a diode-like behavior. The SPCM images have furthermore demonstrated that strongly localized photocurrent generation occurs also in CNT networks. These findings provide valuable guidelines for the future design and optimization of CNT network-based devices such as FETs or photodetectors.

Experimental

Random networks of SWCNTs were grown by chemical vapor deposition (CVD) at 800 °C using ethanol as carbon feedstock. Prior to the growth, iron catalysts were wet-chemically prepared on highly doped n⁺-Si substrates with a 200 nm thick thermally grown SiO₂ layer. Nanotube

networks with specific dimensions were obtained by utilizing a lithographically defined mask to protect an area with approximate dimensions of $8\ \mu\text{m} \times 20\ \mu\text{m}$ during etching by oxygen plasma. Standard electron-beam lithography was used to define Ti/AuPd (0.3 nm / 15 nm) electrodes on top of the SWCNTs. SPCM was carried out with a diffraction-limited HeNe laser spot ($\lambda \approx 633\ \text{nm}$, $E \approx 1.96\ \text{eV}$, spot size $\approx 0.5\ \mu\text{m}$, laser intensity $\approx 100\ \text{kW cm}^{-2}$) from a Leica TCS SP2 confocal microscope [9]. While the sample was scanned through the laser spot with the aid of a piezo stage, the drain current and the reflected light were recorded as a function of the laser spot position, yielding photocurrent and optical images, respectively. By adjusting the back gate voltage, photocurrent images were obtained in different transport regimes (i.e., p-type ON, OFF, or n-type ON). All measurements were performed under ambient conditions and the images analyzed using the WSxM package [16].

Acknowledgements

The authors thank Nan Fu and Alf Mews (University of Siegen) for providing carbon nanotubes synthesized by CVD. Supporting Information is available online from Wiley InterScience or from the authors.

Received: December 1, 2008

Revised: February 12, 2009

Published online: April 20, 2009

- [1] *Introducing Molecular Electronics* (Eds: G. Cuniberti, G. Fagas, K. Richter,), Lecture Notes in Physics, Vol. 680, Springer, Berlin 2005.
- [2] a) S. J. Tans, A. R. M. Verschueren, C. Dekker, *Nature* **1998**, 393, 49. b) R. Martel, T. Schmidt, H. R. Shea, T. Hertel, P. Avouris, *Appl. Phys. Lett.* **1998**, 73, 2447. c) P. Avouris, Z. H. Chen, V. Perebeinos, *Nat. Nanotechnol.* **2007**, 2, 605.
- [3] a) M. C. Hersam, *Nat. Nanotechnol.* **2008**, 3, 387. b) R. Krupke, F. Hennrich, *Adv. Eng. Mater.* **2005**, 7, 111.
- [4] a) E. S. Snow, J. P. Novak, P. M. Campbell, D. Park, *Appl. Phys. Lett.* **2003**, 82, 2145. b) S. J. Kang, C. Kocabas, T. Ozel, M. Shim, N. Pimparkar, M. A. Alam, S. V. Rotkin, J. A. Rogers, *Nat. Nanotechnol.* **2007**, 2, 230. c) M. C. Lemieux, M. Roberts, S. Barman, Y. W. Jin, J. M. Kim, Z. Bao, *Science* **2008**, 321, 101. d) L. Hu, D. S. Hecht, G. Grüner, *Nano Lett.* **2004**, 4, 2513.
- [5] a) K. Bradley, J. C. P. Gabriel, G. Grüner, *Nano Lett.* **2003**, 3, 1353. b) Q. Cao, H. Kim, N. Pimparkar, J. P. Kulkarni, C. Wang, M. Shim, K. Roy, M. A. Alam, J. A. Rogers, *Nature* **2008**, 454, 495.
- [6] a) A. Fujiwara, Y. Matsuoka, H. Suematsu, N. Ogawa, K. Miyano, H. Kataura, Y. Maniwa, S. Suzuki, Y. Achiba, *Jpn. J. Appl. Phys.* **2001**, 40, L1229. b) A. Fujiwara, Y. Matsuoka, Y. Matsuoka, H. Suematsu, N. Ogawa, K. Miyano, H. Kataura, Y. Maniwa, S. Suzuki, Y. Achiba, *Carbon* **2004**, 42, 919. c) E. Adam, C. M. Aguirre, L. Marty, B. C. St-Antoine, F. Meunier, P. Desjardins, D. Ménard, R. Martel, *Nano Lett.* **2008**, 8, 2351.
- [7] M. S. Fuhrer, J. Nygard, L. Shih, M. Forero, Y. G. Yoon, M. S. C. Mazzoni, H. J. Choi, J. Ihm, S. G. Louie, A. Zettl, P. L. McEuen, *Science* **2000**, 288, 494.
- [8] a) D. H. Kim, J. Huang, H. K. Shin, S. Roy, W. Choi, *Nano Lett.* **2006**, 6, 2821. b) L. W. Liu, J. H. Fang, L. Lu, F. Zhou, H. F. Yang, A. Z. Jin, C. Z. Gu, *Phys. Rev. B* **2005**, 71, 155424.
- [9] a) K. Balasubramanian, Y. Fan, M. Burghard, K. Kern, M. Friedrich, U. Wannek, A. Mews, *Appl. Phys. Lett.* **2004**, 84, 2400. b) K. Balasubramanian, M. Scolari, A. Mews, M. Burghard, K. Kern, *Nano Lett.* **2005**, 5, 507.
- [10] a) E. J. H. Lee, K. Balasubramanian, J. Dorfmueller, R. Vogelgesang, N. Fu, A. Mews, M. Burghard, K. Kern, *Small* **2007**, 3, 2038. b) M. Freitag, J. C. Tsang, A. Bol, D. N. Yuan, J. Liu, P. Avouris, *Nano Lett.* **2007**, 7, 2037. c) Y. H. Ahn, A. W. Tsen, B. Kim, Y. W. Park, J. Park, *Nano Lett.* **2007**, 7, 3320.
- [11] In order to maximize the photocurrent to dark-current ratio, biased SPCM measurements were taken in gate voltage ranges around the OFF state of the devices.
- [12] S. Suzuki, Y. Watanabe, Y. Homma, S. Fukuba, S. Heun, A. Locatelli, *Appl. Phys. Lett.* **2004**, 85, 127.
- [13] H. M. Manohara, E. W. Wong, E. Schlecht, B. D. Hunt, P. H. Siegel, *Nano Lett.* **2005**, 5, 1469.
- [14] S. Heinze, J. Tersoff, R. Martel, V. Derycke, J. Appenzeller, P. Avouris, *Phys. Rev. Lett.* **2002**, 89, 106801.
- [15] C. Papadopoulos, A. Rakitin, J. Li, A. S. Vedenev, J. M. Xu, *Phys. Rev. Lett.* **2000**, 85, 3476.
- [16] I. Horcas, R. Fernandez, J. M. Gomez-Rodriguez, J. Colchero, J. Gomez-Herrero, A. M. Baro, *Rev. Sci. Instrum.* **2007**, 78, 013705.